k-t Self-Consistency Diffusion: A Physics-Informed Model for Dynamic MR Imaging

Ye Liu[1,2], Zhuo-Xu Cui[2], Kaicong Sun[1], Ting Zhao[2], Jing Cheng[2], Yuliang Zhu[2,3], Dinggang Shen[1,5,6] (✉), and Dong Liang[1,2,4] (✉)

[1] School of Biomedical Engineering & State Key Laboratory of Advanced Medical Materials and Devices, ShanghaiTech University, Shanghai 201210, China
[2] Shenzhen Institutes of Advanced Technology, Chinese Academy of Sciences, Guangdong, China
[3] University of Nottingham Ningbo China, Zhejiang, China
[4] Key Laboratory of Biomedical Imaging Science and System, Chinese Academy of Sciences, Shenzhen, China
[5] Shanghai United Imaging Intelligence Co., Ltd., Shanghai, China
[6] Shanghai Clinical Research and Trial Center, Shanghai, China
{liuye2022, dgshen}@shanghaitech.edu.cn, {zx.cui, dong.liang}@siat.ac.cn

Abstract. Diffusion models exhibit promising prospects in magnetic resonance (MR) image reconstruction due to their robust image generation and generalization capabilities. However, current diffusion models are predominantly customized for 2D image reconstruction tasks. When addressing dynamic MR imaging (dMRI), the challenge lies in accurately generating 2D images while simultaneously adhering to the temporal direction and matching the motion patterns of the scanned regions. In dynamic parallel imaging, motion patterns can be characterized through the self-consistency of k-t data. Motivated by this observation, we propose to design a diffusion model that aligns with k-t self-consistency. Specifically, following a discrete iterative algorithm to optimize k-t self-consistency, we extend it to a continuous formulation, thereby designing a stochastic diffusion equation in line with k-t self-consistency. Finally, by incorporating the score-matching method to estimate prior terms, we construct a diffusion model for dMRI. Experimental results on a cardiac dMRI dataset showcase the superiority of our method over current state-of-the-art techniques. Our approach exhibits remarkable reconstruction potential even at extremely high acceleration factors, reaching up to 24X, and demonstrates robust generalization for dynamic data with temporally shuffled frames.

Keywords: Diffusion models · Physics-informed deep learning · k-t self-consistency · MR reconstruction.

Y. Liu and Z. Cui—Contributed equally to this work.

1 Introduction

Dynamic Magnetic Resonance Imaging (dMRI) is a powerful imaging modality due to its superior spatial resolution and ability to reveal temporal motion. However, the inherent long acquisition time of dMRI [12] scans renders MR images vulnerable to motion artifacts [3,7] and limits their spatial and temporal resolutions. Therefore, undersampling data and incorporating physical priors for accelerated imaging have emerged as a prominent research focus. Given the distinctive imaging attributes, dynamic imaging acceleration is required to incorporate priors in spatial (k) and temporal (t) dimensions.

To leverage k-t priors for connecting spatiotemporal correlations, early researches integrated compressed sensing (CS) [15] into MR reconstruction, resulting in promising outcomes. k-t SLR [13] and L+S [17] utilize sparse and low-rank constraints in different dimensions. However, due to the challenges associated with hyperparameters selection and long reconstruction times, researchers have turned to utilizing deep networks to transform CS methods into deep learning-based approaches, such as PS-Net [5] and [6]. These methods employ complex 2D+1D networks for reconstruction, where the 2D network encodes spatial priors and the 1D network models temporal dynamics. Common implementations include 3D convolutions [11,23], 2D+1D convolutions [21], and CRNN [19,20]. Nevertheless, these approaches are commonly restricted to specific data types.

Recently, score-based diffusion models [24] have demonstrated significant advantages in image generation by using stochastic differential equations (SDE) to encode and decode images across multiple time steps. Compared to traditional deep learning-based methods, diffusion models offer acceleration-independent training [18] and achieve higher acceleration factors [8,4]. However, their primary application is limited to 2D reconstruction, potentially leading deviations from temporal motion patterns in dMRI. [14] introduced an accelerating T1rho diffusion model based on joint distribution, but it struggles to generalize to different data motion patterns.

In response to the limitations of diffusion in dMRI, we propose a diffusion model that ensures the generated images conform to the motion patterns in the temporal direction. Specifically, we extend the k-t self-consistency discrete iterative algorithm to a continuous paradigm, and design the drift and diffusion coefficient for a novel SDE that satisfies k-t self-consistency of data. Additionally, leveraging the score matching method and SDE with physical priors, we construct a diffusion model that can accurately capture the motion patterns of the scanned region employing k-t self-consistency. To the best of our knowledge, this is the first work to utilize SDE for connecting spatiotemporal information. We evaluated our proposed method on a cardiac dataset, and the results demonstrate its remarkable reconstruction effectiveness at 4 different acceleration factors. Furthermore, when shuffling the temporal frames of the data, our method showed minimal loss, highlighting its strong generalization capabilities.

2 Method

2.1 TSPIRiT

In the paradigm of achieving acceleration through undersampled data acquisition, the imaging process of dMRI can be expressed as:

$$\hat{\mathbf{y}} = \mathbf{A}\mathbf{x} + \mathbf{n}, \tag{1}$$

where $\hat{\mathbf{y}} \in \mathbb{C}^{n_x \times n_y \times n_c \times n_t}$ is the acquired k-space measurements in the dimensions of 2D space, coil, and temporal frame. $\mathbf{x} \in \mathbb{C}^{n_x \times n_y \times n_t}$ is the real image, and $\mathbf{n}$ is the noise interference. The encoding matrix $\mathbf{A} = \mathbf{M}\mathbb{F}\mathbf{S}$ includes coil sensitivity map (CSM) $\mathbf{S}$, Fourier operator $\mathbb{F}$ and sampling mask $\mathbf{M}$.

SPIRiT [16] is a static imaging method with k-c physical self-consistency that utilizes coil-by-coil relationships for k-space data interpolation reconstruction. According to [9,10], we derived the low-rank property between frames [with details in Appendix]. Consequently, we can develop TSPIRiT with k-t self-consistency to perform spatiotemporal interpolation based on SPIRiT.

The schematic of TSPIRiT is shown in Fig. 1(a), which implements k-t self-consistency by utilizing the neighboring 2D+t space (including acquired and unacquired points) to interpolate until the synthesized data $\mathrm{G}\hat{\mathbf{x}}$ from neighboring points and $\hat{\mathbf{x}}$ are equal. The optimization equation can be modeled as:

$$\arg\min_{\hat{\mathbf{x}}} ||\mathbf{G}\hat{\mathbf{x}} - \hat{\mathbf{x}}||_2^2, \quad s.t.\ ||\mathbf{A}\mathbf{x} - \hat{\mathbf{y}}||_2^2 \leq \epsilon, \tag{2}$$

where the first term enforces self-consistency of data, and the second term realizes the consistency with the MR physical imaging. The kernel G is a weight matrix obtained from the calibration region [16] and operates on the 2D+t space to fill in the missing data points. $\hat{\mathbf{x}} = \mathbb{F}\mathbf{x}$ is the interpolation result in k-space, and ϵ is used to control the degree of data consistency.

2.2 k-t Self-Consistency Diffusion

TSPIRiT-SDE To avoid learning inherent spatiotemporal relationships using deep networks, we consider modeling a SDE with k-t self-consistency through the interpolation process of TSPIRiT. Specifically, let $\mathbf{x}_0$ be the recovered image, the discrete iterative algorithm of Eq. 2 is described as:

$$\mathbf{x}_k = \mathbf{x}_{k+1} + \alpha_{k+1}\Phi(\mathbf{x}_{k+1}) + \beta_{k+1}\mathbf{A}^H(\mathbf{A}\mathbf{x}_{k+1} - \hat{\mathbf{y}}), \quad k = T-1, \ldots, 0, \tag{3}$$

where α and β are used to control steps, $\Phi(\mathbf{x}) = \mathbb{F}^{-1}(\mathbf{G} - \mathbf{I})^H(\mathbf{G} - \mathbf{I})\mathbb{F}\mathbf{x}$ represents the gradient of the self-consistency term. The interpolation process can be seen as the reverse diffusion process conditioned on $\mathbf{A}\mathbf{x} - \hat{\mathbf{y}}$ without generation capability. Consequently, based on the continuous formulation of Eq. 3, Φ can be regarded as the drift coefficient of SDE. Moreover, considering the high similarity between frames, adding the same Gaussian noise to different frames, the model may struggle to discriminatively reconstruct them. Thus, we propose

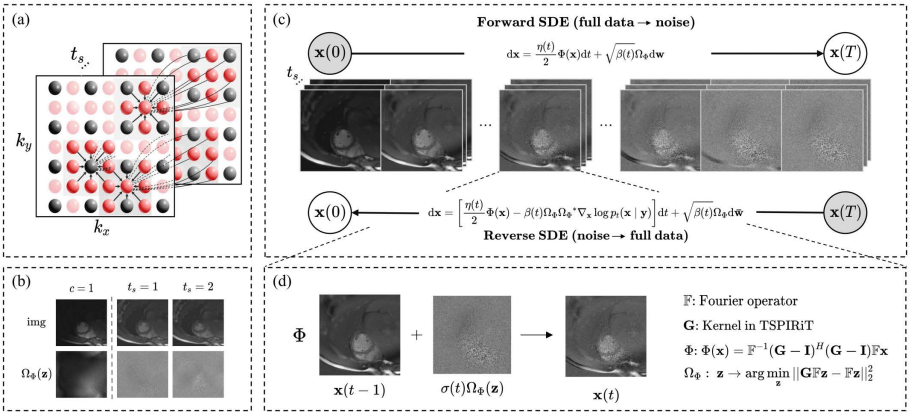

Fig. 1. (a) TSPIRiT: k-space interpolation in the adjacent 2D+t space (black and red points denote acquired and missing data). (b) The self-consistency constraint effect of Ω_Φ on coil (the first column) and temporal dimension (the second and third columns). (c) The overall framework of k-t Self-Consistency Diffusion. (d) The detailed forward process of self-consistency noise is gradually injected into the multi-frame images.

Ω_Φ with k-t self-consistency to constrain noises that conform to image motion patterns. The constraint process is defined as:

$$\Omega_\Phi: \ \mathbf{z} \rightarrow \arg\min_{\mathbf{z}} ||\mathbf{G}\mathbb{F}\mathbf{z} - \mathbb{F}\mathbf{z}||_2^2, \ \ \forall \mathbf{z} \in \mathbb{C}^{n_x * n_y * n_t}, \tag{4}$$

where $\mathbf{z}$ is initialized from $\mathcal{N}(0, \mathrm{I})$. The constraint effect is illustrated in Fig. 1(b). For better illustration, we also present the constraint performance on coil dimension based on SPIRiT. Ultimately, we derive the novel TSPIRiT-SDE in line with k-t self-consistency:

$$\mathrm{d}\mathbf{x} = \frac{\eta(t)}{2}\Phi(\mathbf{x})\mathrm{d}t + \sqrt{\beta(t)}\Omega_\Phi \mathrm{d}\mathbf{w}. \tag{5}$$

According to the theory of SDE [2], there exists a reverse SDE for Eq. 5 enabling the reconstruction. Specifically, we derive the reverse SDE as:

$$\mathrm{d}\mathbf{x} = \left[\frac{\eta(t)}{2}\Phi(\mathbf{x}) - \beta(t)\Omega_\Phi {\Omega_\Phi}^* \nabla_{\mathbf{x}} \log p_t(\mathbf{x} \mid \mathbf{y})\right]\mathrm{d}t + \sqrt{\beta(t)}\Omega_\Phi \mathrm{d}\bar{\mathbf{w}}. \tag{6}$$

Estimating the Score Function It is crucial to obtain the perturbation kernel of SDE to estimate $\nabla_{\mathbf{x}} \log p_t(\mathbf{x} \mid \mathbf{y})$. According to Eq. 5.50 and 5.51 in [22], we derive the perturbation kernel of the proposed SDE (with details in Appendix):

$$p_{0t}(\mathbf{x}(t) \mid \mathbf{x}(0) = \mathcal{N}(\mathbf{x}(t); \mathbf{x}(0), \sigma^2 \Omega_\Phi \Omega_\Phi^*(\mathbf{I})), \tag{7}$$

the score function of the proposed model is derived as:

$$\theta^* = \arg\min_\theta \mathbb{E}_t\{\lambda(t)\mathbb{E}_{\mathbf{x}(0)}\mathbb{E}_{\mathbf{x}(t)|\mathbf{x}(0)}[||\sigma \mathbf{s}_\theta(\mathbf{x}(t), t) + \Omega_\Phi(\mathbf{z})||_2^2]\}. \tag{8}$$

Algorithm 1 PC Sampling (TSPIRiT-SDE).

Require: $\{\eta_i\}_{i=1}^N$, $\{\beta_i\}_{i=1}^N$, σ, λ_1, λ_2, r, K, N, $\hat{\mathbf{y}}$, $\mathbf{S}$, $\mathbf{M}$

Initialize $\mathbf{x}_N \sim \Omega_\Phi(\mathcal{N}(0, \sigma^2))$, $\mathbf{z} \sim \Omega_\Phi(\mathcal{N}(0, \mathrm{I})$
for $i = N-1$ **to** 0 **do**
  $\mathbf{g} \leftarrow s_{\theta^*}(\mathbf{x}_{i+1}, i+1)$
  $\mathbf{m} = \sum_{c=1}^{n_c} \mathbf{S}_c^* \mathbb{F}^{-1} \left(\mathbb{F}(\mathbf{S}_c \mathbf{x}_i)\mathbf{M} - \hat{\mathbf{y}}\right)$
  $\epsilon \leftarrow \lambda_1 \left(||\mathbf{g}||_2 / ||\mathbf{m}||_2\right)$
  $\mathbf{x}_i \leftarrow \mathbf{x}_{i+1} + \frac{1}{2}\eta_{i+1}\Phi(\mathbf{x}_{i+1}) + \beta_{i+1}\Omega_\Phi(\mathbf{g} - \epsilon\mathbf{m}) + \sqrt{\beta_{i+1}}\Omega_\Phi(\mathbf{z})$
  for $k \leftarrow 1$ **to** K **do**
    $\mathbf{g} \leftarrow s_{\theta^*}(\mathbf{x}_i^{k-1}, i)$
    $\mathbf{m} = \sum_{c=1}^{n_c} \mathbf{S}_c^* \mathbb{F}^{-1} \left(\mathbb{F}(\mathbf{S}_c \mathbf{x}_i^k)\mathbf{M} - \hat{\mathbf{y}}\right)$
    $\epsilon_1 \leftarrow 2\left(r||\mathbf{z}||_2 / ||\mathbf{g}||_2\right)^2$
    $\epsilon_2 \leftarrow \lambda_2 \left(||\mathbf{g}||_2 / ||\mathbf{m}||_2\right)$
    $\mathbf{x}_i^k \leftarrow \mathbf{x}_i^{k-1} + \frac{1}{2}\eta_{i+1}\mathbf{x}_i^{k-1} + \epsilon_1(\mathbf{g} - \epsilon_2\mathbf{m}) + \sqrt{2\epsilon_1}\Omega_\Phi(\mathbf{z})$
  end for
  $\mathbf{x}_{i-1} \leftarrow \mathbf{x}_i^K$
end for
return $\mathbf{x}_0$ ▷ $\mathbf{x}_i = \mathbf{x}_i^0$

The framework of k-t Self-Consistency Diffusion is shown in Fig. 1, and Predictor-Corrector (PC) sampling for image generation is presented in Algorithm 1.

3 Experiments and Results

3.1 Dataset

The fully sampled dMRI data were acquired using a 3T MR scanner (MAGNETOM Trio, Siemens) with 20-channel receiver coil arrays. Imaging parameters used for data acquisition were: TE/TR = 1.5/3.0 ms, FOV = 330×330 mm, slice thickness = 6 mm, acquisition matrix = 256×256. The data were collected from 29 volunteers with 356 slices, among which 25 randomly selected patients were used for training, and the remaining 4 were used for testing. We applied rigid transformation-shearing for data augmentation, shearing the dynamic images in the x, y, and t directions. Eventually, we obtained 800 2D-t multi-coil cardiac samples sized 192 × 192 × 18 ($n_x \times n_y \times n_t$) for training, and 118 samples for testing. In the experiments, random Cartesian undersampling masks [1] were used to create sample pairs, and CSM were estimated by ESPIRiT [25].

3.2 Implementation Details

Compared to other methods using 2D+1D networks to capture motion patterns, our method utilizes the 2D ncsnpp network [24] of VE-SDE. The temporal frame is rearranged to the batch size dimension to ensure consistency in the convolution parameters of each frame. Therefore, the input tensor has a size of $n_t \times 2 \times n_x \times n_y$, where 2 represents the concatenated real and imaginary parts of the complex

data. The training procedure consisted of over 200 epochs, the ADAM optimizer was used to train the model, and the exponential moving average (EMA) rate was set to 0.999. The numbers of iterations N and K were set to 1000 and 1. The conjugate gradient descent algorithm with 5 iterations was utilized to quickly solve the optimization equation in Eq. 4.

3.3 Comparison with State-of-the-Art Methods

We compared our method with state-of-the-art reconstruction methods, including TSPIRiT, CS method L+S [17], deep learning-based DL-ESPIRiT [21], and score-based methods (VE-SDE [8] and Joint-VE-SDE [14]). Particularly, VE-SDE and Joint-VE-SDE were used to verify the effectiveness of the proposed SDE for temporal information interaction.

Table 1. Quantitative comparison of different methods with 4 acceleration factors.

ACC	Method	MSE(∗e-5)	PSNR	SSIM(∗e-2)
12X	TSPIRiT	41.87 ± 20.38	34.22 ± 1.89	91.82 ± 3.34
	L+S	22.68 ± 17.21	37.35 ± 2.66	93.14 ± 2.72
	DL-ESPIRiT	5.49 ± 2.96	43.15 ± 2.14	96.73 ± 1.25
	VE-SDE	145.28 ± 156.34	31.18 ± 5.22	84.49 ± 5.63
	Joint-VE-SDE	16.59 ± 33.81	42.36 ± 4.78	96.42 ± 2.23
	Ours	**2.83 ± 2.15**	**46.42 ± 2.74**	**98.15 ± 0.90**
16X	TSPIRiT	51.52 ± 27.48	33.35 ± 1.94	89.43 ± 4.04
	L+S	49.98 ± 33.75	33.84 ± 2.65	88.07 ± 4.62
	DL-ESPIRiT	8.03 ± 3.90	41.42 ± 1.98	95.67 ± 1.43
	VE-SDE	191.13 ± 170.59	29.08 ± 4.29	78.46 ± 7.08
	Joint-VE-SDE	13.68 ± 33.80	41.57 ± 4.03	96.32 ± 2.13
	Ours	**6.34 ± 3.86**	**44.54 ± 3.28**	**97.65 ± 1.12**
20X	TSPIRiT	55.19 ± 24.93	32.95 ± 1.72	88.84 ± 3.80
	L+S	113.44 ± 49.88	29.88 ± 1.96	80.56 ± 5.37
	DL-ESPIRiT	11.28 ± 5.23	39.91 ± 1.93	94.60 ± 1.56
	VE-SDE	250.27 ± 204.88	27.59 ± 3.91	74.68 ± 7.23
	Joint-VE-SDE	26.03 ± 78.23	41.14 ± 4.66	96.11 ± 1.92
	Ours	**5.04 ± 3.32**	**43.63 ± 2.21**	**97.21 ± 1.06**
24X	TSPIRiT	64.37 ± 25.56	32.20 ± 1.52	86.68 ± 4.15
	L+S	231.99 ± 104.51	26.79 ± 2.00	73.60 ± 5.49
	DL-ESPIRiT	13.26 ± 6.35	39.22 ± 1.93	94.11 ± 1.75
	VE-SDE	489.82 ± 381.14	24.59 ± 3.87	67.78 ± 7.99
	Joint-VE-SDE	63.12 ± 108.48	40.30 ± 4.43	95.39 ± 2.79
	Ours	**6.56 ± 4.15**	**42.45 ± 2.16**	**96.73 ± 1.25**

Table 1 presents the quantitative results of different methods with various acceleration factors. The proposed approach outperforms other methods, even at a high acceleration factor of 24. The visual results depicted in Fig. 2 demonstrate that our method achieves more accurate and detailed reconstruction compared

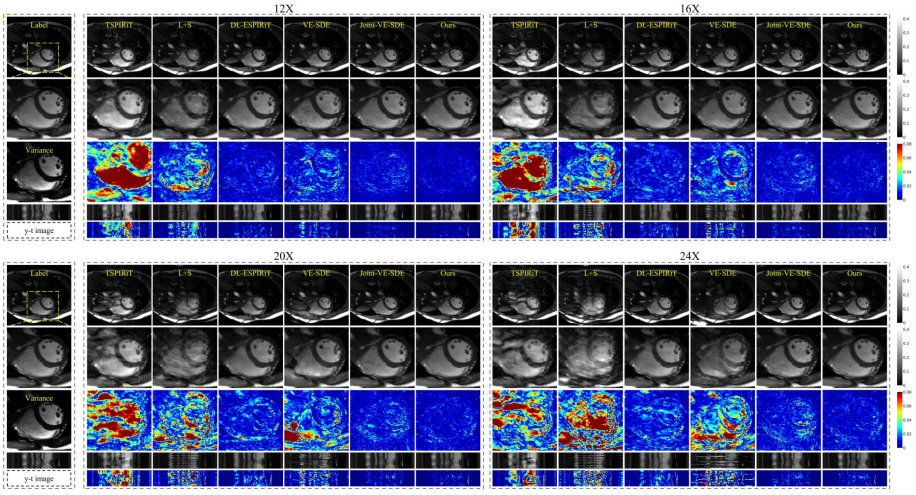

Fig. 2. Visual comparison of different methods with 4 acceleration factors.

to others. Specifically, we also present the reconstruction results of challenging systolic images (see Appendix). The advantages compared to VE-SDE and Joint-VE-SDE highlight the effectiveness of utilizing a 2D network and the proposed SDE with k-t self-consistency for processing three-dimensional (2D+t) data. Both the SDE-based Joint-VE-SDE and our method demonstrate significant advantages over traditional methods at high acceleration factors. However, VE-SDE struggles to generate realistic images at high accelerations due to its inability to utilize temporal correlations effectively. This leads to unstable and unrealistic results, as seen in the high variance of VE-SDE in Table 1.

3.4 Ablation Study

To further verify the effectiveness of the proposed SDE, we conducted experiments to investigate the contributions of the drift coefficient Φ and the self-consistency constraint of noise Ω_Φ. The quantitative and qualitative results with acceleration factors of 12 and 16 are respectively presented in Table 2 and Fig. 3. The results show that the model fails to achieve proper reconstruction without Φ, as our method relies on it for k-t self-consistency reconstruction. And the neglect of the noise constraint term Ω_Φ significantly affects the detail preserving ability, aligning with the purpose of using Ω_Φ to differentiate time frames with high similarity. This highlights that the key point of the proposed k-t Self-Consistency Diffusion in achieving dynamic image reconstruction lies in the k-t consistency embedded in the SDE, rather than complex networks.

Table 2. Quantitative results of ablation study on Φ and Ω_Φ in the proposed SDE with acceleration fators of 12 and 16.

ACC	Method	Φ	Ω_Φ	MSE(∗e-5)	PSNR	SSIM(∗e-2)
12X	w/o Φ	✓		566.22 ± 344.16	23.09 ± 2.23	59.46 ± 7.65
	w/o Ω_Φ		✓	13.35 ± 3.98	38.93 ± 1.24	89.29 ± 2.00
	Ours	✓	✓	**2.83 ± 2.15**	**46.42 ± 2.74**	**98.15 ± 0.90**
16X	w/o Φ	✓		688.76 ± 426.39	22.26 ± 2.26	56.87 ± 8.08
	w/o Ω_Φ		✓	48.71 ± 36.94	34.24 ± 3.18	78.16 ± 8.34
	Ours	✓	✓	**6.34 ± 1.86**	**44.54 ± 3.28**	**97.65 ± 1.12**

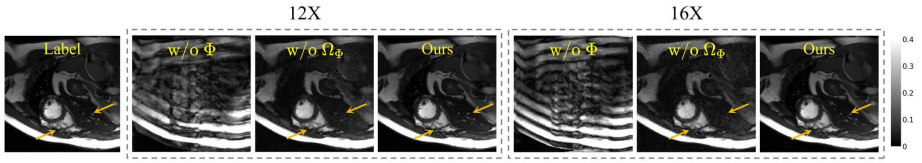

Fig. 3. Visual results of ablation study on Φ and Ω_Φ in the proposed SDE with acceleration fators of 12 and 16.

3.5 Performance on Temporally-Frame-Shuffled Data

To evaluate the generalization of the proposed method, we randomly shuffled the temporal frame order of data and compared our method with Joint-VE-SDE, the well-performing SDE-based method with competent reconstruction capabilities. The experimental results before and after two different random shufflings are shown in Fig. 4. The results indicate that the arrangement of temporal frames in dynamic MR images has minimal impact on our model, while Joint-VE-SDE exhibits poor reconstruction performance after shuffling. This is because our method leverages SDE to facilitate inter-frame information interaction, instead of relying on networks like Joint-VE-SDE to directly learn temporal patterns. This advantage is particularly beneficial for imaging irregular dynamic movements.

4 Conclusion and Discussion

In this study, we developed a novel diffusion model with k-t self-consistency based on a SDE that can conform the dynamic patterns of dMRI data in the 2D+t space. This model eliminates the need for complex networks and instead utilizes a continuous paradigm inspired by the discrete iterative process of TSPIRiT. By incorporating k-t self-consistency, our SDE can effectively track information in the temporal dimension, allowing us to design the diffusion model based on score-matching theory. Experimental results on cardiac datasets have demonstrated the effectiveness and generalization of our approach. In future research, we intend to explore the potential application of this model in reconstructing other irregular dynamic data.

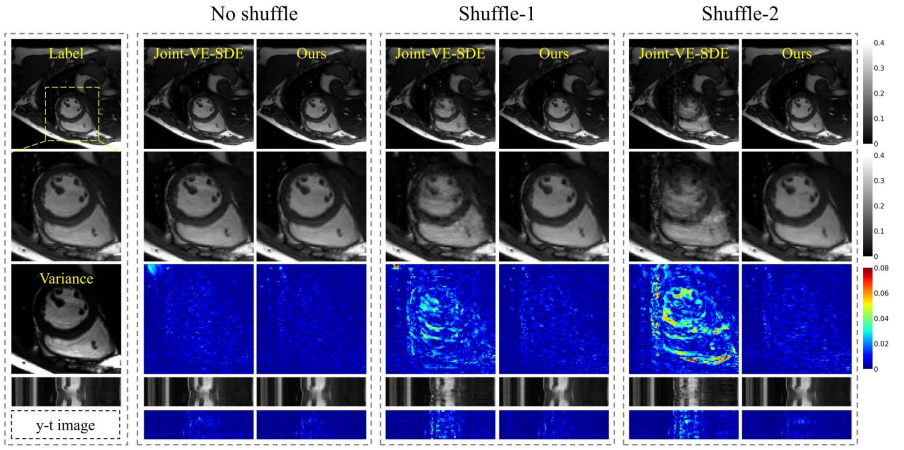

Fig. 4. Results of diffusion-based models on temporally shuffled data at R = 12.

Acknowledgments. This study was funded by the National Natural Science Foundation of China (62131015, 62250710165, U23A20295, 62106252, 62331028, 62206273 and 62125111), and Key Laboratory for Magnetic Resonance and Multimodality Imaging of Guangdong Province (2023B1212060052).

Disclosure of Interests. The authors have no competing interests to declare that are relevant to the content of this article.

References

1. Ahmad, R., Xue, H., Giri, S., Ding, Y., Craft, J., Simonetti, O.P.: Variable density incoherent spatiotemporal acquisition (vista) for highly accelerated cardiac mri. Magnetic resonance in medicine **74**(5), 1266–1278 (2015)
2. Anderson, B.D.: Reverse-time diffusion equation models. Stochastic Processes and their Applications **12**(3), 313–326 (1982)
3. Bluemke, D.A., Boxerman, J.L., Atalar, E., McVeigh, E.R.: Segmented k-space cine breath-hold cardiovascular mr imaging: Part 1. principles and technique. AJR. American journal of roentgenology **169**(2), 395–400 (1997)
4. Cao, C., Cui, Z.X., Wang, Y., Liu, S., Chen, T., Zheng, H., Liang, D., Zhu, Y.: High-frequency space diffusion model for accelerated mri. IEEE Transactions on Medical Imaging (2024)
5. Cao, C., Cui, Z.X., Zhu, Q., Liang, D., Zhu, Y.: Ps-net: Deep partially separable modelling for dynamic magnetic resonance imaging. arXiv preprint arXiv:2205.04073 (2022)
6. Cheng, J., Cui, Z.X., Huang, W., Ke, Z., Ying, L., Wang, H., Zhu, Y., Liang, D.: Learning data consistency and its application to dynamic mr imaging. IEEE Transactions on Medical Imaging **40**(11), 3140–3153 (2021)
7. Cheng, J.Y., Hanneman, K., Zhang, T., Alley, M.T., Lai, P., Tamir, J.I., Uecker, M., Pauly, J.M., Lustig, M., Vasanawala, S.S.: Comprehensive motion-compensated

highly accelerated 4d flow mri with ferumoxytol enhancement for pediatric congenital heart disease. Journal of Magnetic Resonance Imaging **43**(6), 1355–1368 (2016)
8. Chung, H., Ye, J.C.: Score-based diffusion models for accelerated mri. Medical image analysis **80**, 102479 (2022)
9. Haldar, J.P., Setsompop, K.: Linear predictability in magnetic resonance imaging reconstruction: Leveraging shift-invariant fourier structure for faster and better imaging. IEEE Signal Processing Magazine **37**(1), 69–82 (2020)
10. Jacob, M., Mani, M.P., Ye, J.C.: Structured low-rank algorithms: Theory, magnetic resonance applications, and links to machine learning. IEEE Signal Processing Magazine **37**(1), 54–68 (2020)
11. Küstner, T., Fuin, N., Hammernik, K., Bustin, A., Qi, H., Hajhosseiny, R., Masci, P.G., Neji, R., Rueckert, D., Botnar, R.M., et al.: Cinenet: deep learning-based 3d cardiac cine mri reconstruction with multi-coil complex-valued 4d spatio-temporal convolutions. Scientific reports **10**(1), 13710 (2020)
12. Liang, Z.P., Boada, F., Constable, R., Haacke, E., Lauterbur, P., Smith, M.: Constrained reconstruction methods in mr imaging. Rev Magn Reson Med **4**(2), 67–185 (1992)
13. Lingala, S.G., Hu, Y., DiBella, E., Jacob, M.: Accelerated dynamic mri exploiting sparsity and low-rank structure: kt slr. IEEE transactions on medical imaging **30**(5), 1042–1054 (2011)
14. Liu, C., Cui, Z.X., Liu, Y., Cao, C., Zhu, Q., Zhu, Y., Wang, H., Liang, D.: Joint distribution modeling for accelerating t1rho reconstruction. In: Proc. of the International Society for Magnetic Resonance in Medicine (ISMRM) Annual Meeting and Exhibition. Abstract Number: 6870 (2023)
15. Lustig, M., Donoho, D., Pauly, J.M.: Sparse mri: The application of compressed sensing for rapid mr imaging. Magnetic Resonance in Medicine: An Official Journal of the International Society for Magnetic Resonance in Medicine **58**(6), 1182–1195 (2007)
16. Lustig, M., Pauly, J.M.: Spirit: iterative self-consistent parallel imaging reconstruction from arbitrary k-space. Magnetic resonance in medicine **64**(2), 457–471 (2010)
17. Otazo, R., Candes, E., Sodickson, D.K.: Low-rank plus sparse matrix decomposition for accelerated dynamic mri with separation of background and dynamic components. Magnetic resonance in medicine **73**(3), 1125–1136 (2015)
18. Peng, C., Guo, P., Zhou, S.K., Patel, V.M., Chellappa, R.: Towards performant and reliable undersampled mr reconstruction via diffusion model sampling. In: International Conference on Medical Image Computing and Computer-Assisted Intervention. pp. 623–633. Springer (2022)
19. Qin, C., Schlemper, J., Caballero, J., Price, A.N., Hajnal, J.V., Rueckert, D.: Convolutional recurrent neural networks for dynamic mr image reconstruction. IEEE transactions on medical imaging **38**(1), 280–290 (2018)
20. Qin, C., Schlemper, J., Duan, J., Seegoolam, G., Price, A., Hajnal, J., Rueckert, D.: k-t next: dynamic mr image reconstruction exploiting spatio-temporal correlations. In: Medical Image Computing and Computer Assisted Intervention–MICCAI 2019: 22nd International Conference, Shenzhen, China, October 13–17, 2019, Proceedings, Part II 22. pp. 505–513. Springer (2019)
21. Sandino, C.M., Lai, P., Vasanawala, S.S., Cheng, J.Y.: Accelerating cardiac cine mri using a deep learning-based espirit reconstruction. Magnetic Resonance in Medicine **85**(1), 152–167 (2021)
22. Särkkä, S., Solin, A.: Applied stochastic differential equations, vol. 10. Cambridge University Press (2019)

23. Schlemper, J., Caballero, J., Hajnal, J.V., Price, A.N., Rueckert, D.: A deep cascade of convolutional neural networks for dynamic mr image reconstruction. IEEE transactions on Medical Imaging **37**(2), 491–503 (2017)
24. Song, Y., Sohl-Dickstein, J., Kingma, D.P., Kumar, A., Ermon, S., Poole, B.: Score-based generative modeling through stochastic differential equations. arXiv preprint arXiv:2011.13456 (2020)
25. Uecker, M., Lai, P., Murphy, M.J., Virtue, P., Elad, M., Pauly, J.M., Vasanawala, S.S., Lustig, M.: Espirit—an eigenvalue approach to autocalibrating parallel mri: where sense meets grappa. Magnetic resonance in medicine **71**(3), 990–1001 (2014)